RSC Advances




ROYAL SOCIETY OF CHEMISTRY

www.rsc.org/advances

RSC Advances

RSCPublishing

ARTICLE

# Development of a Novel Nitrite Electrochemical Sensor by Stepwise in situ Formation of Palladium and Reduced Graphene Oxide Nanocomposites

Li Fu[a], Shuhong Yu[b], Lachlan Thompson[a] and Aimin Yu[a,*]

Cite this: DOI: 10.1039/x0xx00000x

Received 00th January 2012,
Accepted 00th January 2012

DOI: 10.1039/x0xx00000x

www.rsc.org/

In this paper, a novel and sensitive electrochemical nitrite sensor was prepared by in situ electroless deposition of Pd nanoparticles and reduced graphene oxide (RGO) stepwisely on a glassy carbon electrode. The deposition process was very fast and the amount of Pd/RGO deposited on the electrode was well controlled by the number of the deposition cycle. The fabrication process was monitored by UV-vis spectroscopy, and the as prepared composites were characterized by FTIR, Raman spectroscopy, XRD and SEM. The results confirmed the successful formation of Pd and the chemical reduction of graphene oxides. Moreover, the incorporation of Pd in between RGO sheets effectively prevented the agglomeration of RGO. The Pd/RGO modified electrode exhibited significant enhancement to the oxidation of nitrite with increased current response and reduced over-potential which was a result of the synergistic catalytic effect of RGO and Pd nanoparticles. The influence of various experimental parameters on the detection of nitrite was studied in detail. Under optimum conditions, the developed nitrite sensor had a linear response in the concentration range of 1—1000 μM and a detection limit of 0.23 μM. Additionally, the fabricated nitrite sensor showed excellent selectivity, reproducibility and stability.

## 1. Introduction

Quantitative analysis and estimation of nitrite ($NO_2^-$) has attracted increasing attention in the past decades because nitrites can interact with amines to form carcinogenic nitrosamines and oxidize hemoglobin to methemoglobin, which causes health problems known as methemoglobinemia [1, 2]. It is worth noting that nitrite is a substance commonly used as a preservative, dyeing agent, fertilizer and food additive. Therefore, it is necessary to develop reliable methods for the detection and monitoring of nitrite. Till now, several techniques have been established for detecting nitrite, such as spectrophotometry [3], chemiluminescence [4], spectrofluorimetry and electrochemical methods [5-7]. However, most techniques have drawbacks such as using toxic reagents, requiring time-consuming sample preparation process, and suffering of interference effect. Among them, the electrochemical method has attracted increasing attention due to its fast procedure, low cost, low detection limit and high accuracy [8, 9]. However, the electrochemical oxidation of nitrite at most common electrodes suffers large overpotentials. Therefore, the sensitivity and accuracy of the electrode could be inhibited by other electro-active interferences. In order to address this problem, electrode surface modification has been adopted for lowering the oxidation potential and increasing the current response.

Carbon materials are among the most widely-used materials for electrochemical sensing purpose [10-13]. For example, multi-walled carbon nanotubes coupled with Au nanoparticles were used for the sensitive electro-determination of $H_2O_2$ [14]. Studies have shown that graphene based electrodes possess superior electrocatalytic property and conductivity than other carbon based materials [15, 16]. Many reports have demonstrated that coupling graphene with noble metal nanoparticles could further enhance its electrocatalytic performance [17-19]. In particular, Pd nanoparticles have been extensively explored for the determination of various analytes because of its excellent electrocatalytic property [20]. Pd nanoparticle modified electrodes are normally prepared by in situ electro-deposition from a Pd precursor solution or by immobilization of pre-synthesized Pd nanoparticles onto electrodes.

In this work, we propose a fast stepwise fabrication method for in situ depositing Pd nanoparticles and graphene oxide (GO) onto the electrode surface. During the fabrication process, Pd and reduced graphene oxide (RGO) nanocomposites are directly formed on the glassy carbon electrode surface with the aid of a chemical reducing agent. The amount of Pd/RGO is well controlled by the number of the deposition cycle. The fabrication procedure is extremely simple and fast. For example, three bilayers of Pd/RGO can be prepared within 3 minutes. The catalytic activity of the fabricated Pd/RGO modified electrode and its enhancement to the electrochemical oxidation of nitrite are studied in detail.

## 2. Experimental

### *2.1 Chemicals and materials*

$NaBH_4$, $C_6N_6FeK_3$, L-ascorbic acid (99%), dopamine hydrochloride (DA), $PdCl_2$, uric acid and glucose were purchased from Sigma-Aldrich. Graphene oxide (GO) powder was purchased from JCNANO, INC (China). All other chemicals used were analytical grade reagents without further purification. Phosphate buffer solutions (PBS) with various pHs were prepared by mixing 0.1 M $KH_2PO_4$ and $K_2HPO_4$ solution and adjusting to appropriate pHs using 0.1 M NaOH and HCl. Milli-Q water (18.2 MΩ cm) was used throughout the experiments.

### *2.2 Modification of glassy carbon electrode with Pd/RGO*

A glassy carbon electrode (GCE, 3 mm diameter) was polished with 1.0, 0.3 and 0.05 μm alumina slurry, respectively. Then the GCE was cleaned through sonication in ethanol and water until a mirror-like surface was formed. The Pd/RGO was deposited onto GCE through a stepwise dipping process. A GCE was firstly dipped into a $NaBH_4$ solution (0.5 M) for 10 s followed by a $N_2$ blow drying process to remove any excess liquid. GCE was then dipped into a $PdCl_2$ solution (0.01 M) for 10 s and dried with $N_2$. After that, the GCE was dipped into a GO dispersion (1 mg/mL) for another 10s and dried with $N_2$. Finally, the GCE was immersed into a $NaBH_4$ solution again for 10 s and gently rinsed by water. The resulting electrode was denoted as G/Pd/RGO-1. These steps were repeated until a desired amount of material was deposited. The multi-cycle deposited electrode was defined as G/Pd/RGO-n. A schematic diagram of the stepwise procedure for electrode modification is shown in Figure 1. GCE modified with only Pd (defined as G/Pd) or GCE modified with only RGO (defined as G/RGO) were prepared using the same procedure except for skipping the step of immersing electrode into GO dispersion (for G/Pd) or $PdCl_2$ solution (for G/RGO).

### *2.3 Characterization*

The surface morphology of modified electrodes was analyzed by a field emission scanning electron microscope (FESEM, ZEISS SUPRA 40VP). The crystal structure of samples was collected from 5° to 80° in 2θ by a XRD with Cu Kα radiation (D8-Advanced, Bruker). Raman spectroscopy was performed at room temperature using a Raman microscope (Renishaw, inVia) with 514 nm laser light. UV-Vis spectrophotometer of model CARY 3E was used to record the absorption spectra of samples fabricated using the same method except for using quartz slide instead of GCE. Fourier transform infrared (FTIR) spectroscopic studies were carried out with a Nicolet iS5 spectrometer. Samples for SEM, XRD, Raman and UV-vis spectroscopy characterizations were prepared using the same procedure except for using quartz slide instead of GCE. The sample for FTIR characterization was films scratched from the quartz slide.

### *2.4 Electrochemical measurements*

Electrochemical measurements were performed on a CHI430a electrochemical workstation using a three electrode system at room temperature. A Pt wire was used as the counter electrode, and an Ag/AgCl (3 M KCl) served as the reference electrode. The modified GCE was used as the work electrode. The differential pulse voltammetry (DPV) was scanned from 0.6 to 0.9 V and the current was recorded as a function of the potential (pulse amplitude of 20 mV, a pulse width of 50 ms).

## 3. Results and Discussion

### 3.1 *Characterization of Pd/RGO modified electrodes*

In this work, Pd/RGO modified GCE was fabricated by a stepwise electroless deposition process. As illustrated in the schematic diagram (Figure 1), when a $NaBH_4$ treated GCE is inserted into a $PdCl_2$ solution, $PdCl_4^{2-}$ ions are reduced by the surface adsorbed $NaBH_4$ to form Pd nanoparticles (NPs) on the electrode. GO sheets are then adsorbed onto the electrode surface mainly via the Van der Waals interaction. At step 3, the reduction of GO sheets occurs when the electrode is immersed in a $NaBH_4$ solution. The reduction process was evidenced by many tiny bubbles appeared on the GCE surface. As each deposition step only takes about 10 s, this electroless deposition process is fast and can be repeated to achieve the desired amount of materials deposited on an electrode.

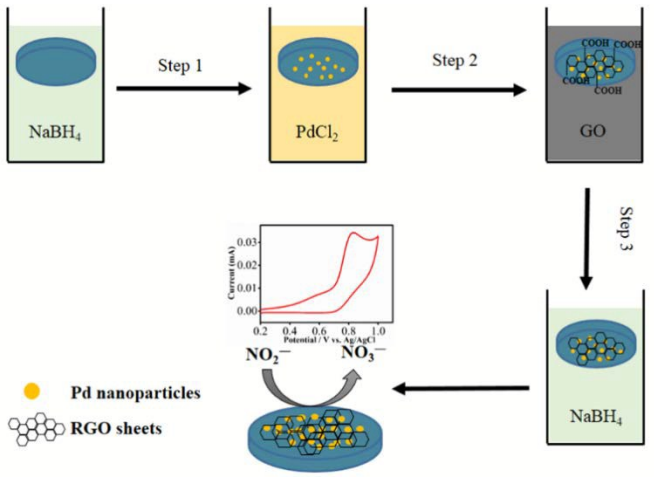


Figure 1. Schematic illustration of the stepwise fabrication of G/Pd/RGO.

In order to confirm the successful formation of Pd/RGO nanocomposites, UV-vis spectroscopy was used to monitor the fabrication process on a quartz slide. As shown in Figure 2A, the GO dispersion exhibits a main absorption peak at 228 nm corresponding to the C=C bond in an aromatic ring [21]. After the dipping process, the spectrum of Pd/RGO shows an absorption peak at 262 nm, which belongs to the absorption of reduced GO sheets. The red-shift from 228 to 262 nm is due to the increase of π-conjugated domains and the formation of a highly conjugated graphite-like structure, which indicating the reduction of GO sheets [22, 23]. It is observed that the absorbance of Pd/RGO composites has a continuous elevation along with the increasing deposition cycle, indicating a regular stepwise growth of the multilayer coating. The plot of Figure 2A inset shows that the absorbance at 262 nm increases linearly with the fabrication cycle number, proving that nearly equal amount of RGO was deposited at each cycle.

Raman scattering is highly sensitive to the electronic structure change of carbon, Raman spectroscopy was thus employed to further characterize the reducing state of GO in the Pd/RGO composite. As shown in Figure 2B, the spectra of GO and Pd/RGO composite both



 

have two main Raman peaks at 1595 (G band) and 1348 $cm^{-1}$ (D band). The intensity ratio of the D and G peaks ($I_D/I_G$) is usually used for analysing the defect concentration and the alignment of the graphitic planes of the carbon based materials [24]. It can be seen that, the $I_D/I_G$ ratio increases from 0.91 (GO) to 1.04 (Pd/RGO composite), which implies the reduction of GO [25, 26]. Moreover, the reduction of GO was further evidenced by FTIR analysis. Figure S1 depicts the FTIR spectra of GO and Pd/RGO composite. The spectrum of GO displays several absorption peaks corresponding to the oxygen-containing groups. The broad band at 3390 $cm^{-1}$ is corresponded to the stretching of O—H. The bands at 1716 and 1616 $cm^{-1}$ are assigned to the stretching of C=O of carbonyl and carboxylic groups, respectively [27]. The bands at 1398 and 1047 $cm^{-1}$ are assigned to the C—OH stretching vibrations and C—O vibrations from alkoxy groups, respectively [28]. However, those peaks are significantly reduced or even vanished in the Pd/RGO composite, strongly indicating that the GO was reduced by dipping into $NaBH_4$ solution.

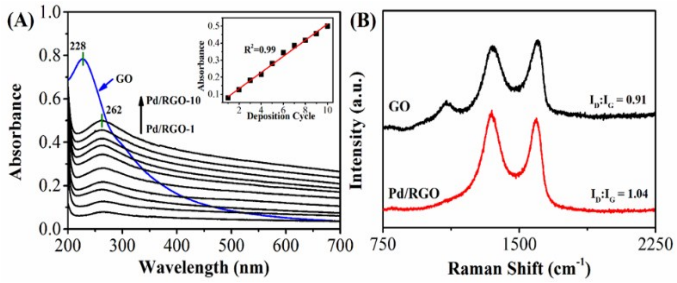


Figure 2. (A) UV-vis spectra of GO dispersion and Pd/RGO deposited quartz slide from 1 to 10 fabrication cycles. Inset shows the plot of absorbance at 262 nm versus the deposition cycle number. (B) Raman spectra of GO and the as prepared Pd/RGO nanocomposite.

Figure 3 shows the top-view SEM images of Pd and Pd/RGO composites prepared by the stepwise dipping method. It can be observed that Pd nanoparticles do not have a defined spherical shape and show small cluster morphology (Figure 3A). For Pd/RGO composite (Figure 3B), well-defined RGO sheets could be observed in a wrinkled shape. Some Pd nanoparticles were embedded under the RGO sheets and exhibit various sized protuberances due to the stepwise fabrication sequence. Under higher magnification, the overlap junction of two fabrication cycles was observed. The RGO sheets did not show an agglomeration in the composite (which usually happens after the reduction of GO) due to the introduction of Pd between the RGO sheets. Therefore, the Pd/RGO composite prepared by stepwise dipping fabrication method has a higher surface area, which is beneficial for the electrochemical sensor development.

The crystalline nature of the Pd/RGO composite was investigated by XRD and the obtained XRD pattern is presented in Figure S2. As seen in Figure S2, the Pd/RGO composite exhibits characteristic diffraction peaks centered at 38.26°, 44.25°, 64.49° and 76.97°, which are assigned to the (111), (200), (222) and (311) crystal facets, indexing face centered cubic Pd (JCPDS 5-681). The small broad diffraction peak centered at 26.80° is related to the graphene sheets. The weak signal indicates that the RGO sheets presented in the composite are exfoliated due to the stepwise dipping fabrication method.

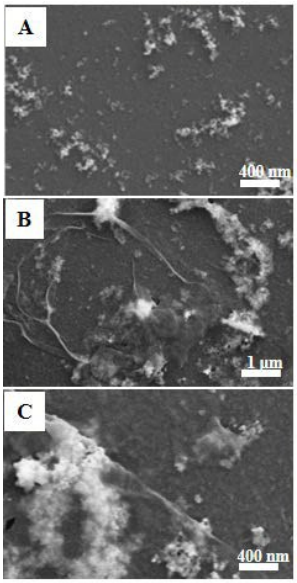


Figure 3. SEM images of Pd nanoparticles (A) and Pd/RGO composite at lower (B) and higher (C) magnification.

The electrochemical behavior of bare GCE, and G/Pd, G/RGO as well as G/Pd/RGO-3 deposited electrodes were investigated and compared using $[Fe(CN)_6]^{4-}$ as an electrochemical probe. Figure S3 depicts the cyclic voltammograms (CVs) of these electrodes in 1 mM $[Fe(CN)_6]^{4-}$ solution containing 0.1 M KCl. Well-defined redox peaks were observed at all electrodes. However, the peak currents of modified electrodes were higher than that at bare GCE, indicating that the modification of either RGO sheets or Pd nanoparticles could enhance the redox reaction of $[Fe(CN)_6]^{4-}$ by increasing the effective surface area and electrical conductivity. Moreover, among those electrodes, the G/Pd/RGO-3 showed the highest current response towards the redox of $[Fe(CN)_6]^{4-}$ probably due to the synergetic effect of Pd nanoparticles and RGO sheets. The electrochemical behavior of bare GCE, G/Pd, G/RGO and G/Pd/RGO-3 were also characterized in pH 7.0 PBS. As shown in Figure S4, no perceptible redox peaks are observed in CVs of G/RGO and bare GCE, indicating that RGO does not undergo redox reaction in the potential range from –0.7 to 0.7 V. In contrast, the CVs of G/Pd and G/Pd/RGO-3 exhibit a oxidation peak at –0.40 and a reduction peak at –0.04 V, corresponding to the redox process of Pd nanoparticles. Furthermore, the redox current of G/Pd/RGO-3 is higher than that of G/Pd, indicating a superior electrochemical activity of the G/Pd/RGO-3 nanocomposite. The enhanced electrochemical activity should be ascribed to the introduction of RGO sheets, which provide a higher surface area for loading Pd nanoparticles.

### *3.2 Electrochemical behavior of nitrite at Pd/RGO modified electrodes*

Figure 4A depicts the CVs of bare GCE, and G/RGO, G/Pd and G/Pd/RGO-3 modified electrodes towards the oxidation of 1 mM nitrite. In the potential range of 0.2—1.0 V, bare GCE does not show any redox peak. At the G/RGO, G/Pd and G/Pd/RGO-3 modified electrodes, a distinct anodic peak corresponding to the oxidation of nitrite is observed. The oxidation peak potentials of nitrite at G/RGO, G/Pd and G/Pd/RGO-3 electrodes were measured to be 0.906, 0886 and 0.829 V, slowly shifting to the more negative potential range. Moreover, the G/Pd/RGO-3 shows a much higher peak current compared to other electrodes. The shift of anodic peak to a more

negative potential and the higher current response reveals that the G/Pd/RGO-3 is an effective promoter to enhance the kinetics of the electrochemical process of nitrite [29].

The influence of the layer of Pd/RGO on the electrocatalytic activity of the electrode was investigated. Figure 4B displays the CV profiles of nitrite oxidation at electrodes deposited with G/Pd/RGO from 1 to 6 fabrication cycles. It can be seen that the anodic peak current increases with increasing deposition cycle till three bilayers. After that, the current response decreases upon further increasing of the deposition cycle. As the reaction of nitrite at the electrode is a diffusion controlled process (see below), the phenomena are probably due to the diffusion effect, that is, it takes longer for nitrite to transfer through the relatively thicker Pd/RGO layers to reach the electrode surface and some Pd nanoparticles inside the inner layers would become difficult to access [30, 31]. Therefore, stepwise dipping fabrication is an effective method for finding the balance between the amount of modification material and the diffusion barrier. Herein G/Pd/RGO-3 with three cycles of deposition had the best performance and was chosen for further experiments.

Figure 4C shows the chronoamprmetric response of G/Pd/RGO-3 in 0.1 mM of nitrite solution when a potential of 0.85 V was applied. A straight line plot of the current against minus square root of time was deduced (Inset of Figure 4C), confirming that the oxidation of nitrite is a diffusion controlled process.

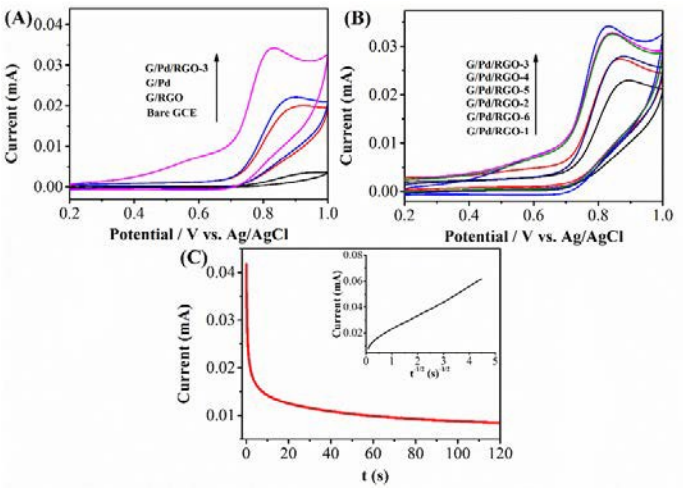


**Figure 4.** Cyclic voltammograms of (A) bare GCE, G/RGO, G/Pd and G/Pd/RGO-3 (B) G/Pd/RGO-1 to G/Pd/RGO-6 modified electrodes in 1 mM nitrite solution at pH 7. Scan rate: 50 mV/s. (C) Chronoamprmetric response of G/Pd/RGO-3 electrode in 0.1 mM of nitrite solution at potential of 0.85 V. Inset: Plot of I vs $t^{-1/2}$ derived from the chronoamprmetric curve.

The relationship between scan rate and current response of nitrite oxidation was investigated. Figure 5A displays the CVs of G/Pd/RGO-3 at scan rate from 20 to 150 mV/s in pH 7.0 PBS containing 1 mM nitrite. The results shows that the oxidation current of nitrite is proportional to the square root of scan rate (inset Figure 5A). The liner regression can be determined as: $I_{pa}$ (mA) = 0.00529 $v^{-1/2}$ ($mV^{1/2}/s^{1/2}$) – 0.00757 ($R^2$ = 0.9867). It further confirmed that the overall electrochemical process is diffusion-controlled. It is noted that the oxidation potential of nitrite gradually shifts to the positive potential when the scan rate increases. A linear regression can be obtained between the oxidation potential and the logarithm of scan rate. It can be expressed as: $E_{pa}$ (V) = 0.10729 log $v$ (V/s) + 1.02656 ($R^2$ = 0.9882), which implying a kinetic limitation in the reaction between the redox sites of G/Pd/RGO-3 and nitrite [7]. Based on this linear equation, the number of electron involved in the reaction can be determined by the Laviron's equation [32, 33]:

$$E_p = E^{o'} + (2.303RT/\alpha nF)\log(RTk_o/\alpha nF) + (2.303RT/\alpha nF)\log v$$

Where $E^{0'}$ is the formal redox potential; $R$ is the gas constant; α is the electron transfer coefficient; F is the Faraday's constant and $k_o$ is the standard heterogeneous rate constant of the reaction. As the slope of $E_p$ versus log $v$ is 0.10729, the $\alpha n$ value can be calculated as 0.5512. The $\alpha$ can be determined from the following equation:

$$E_{p/2} - E_p = 1.875(\mathrm{RT}/\alpha \mathrm{F})$$

From the equation, the value of $\alpha$ was calculated to be 0.4767. Therefore, the number of electron involves in the oxidation of nitrite was determined to be 1.15 ≈ 1, which is in good agreement with previous reports [7, 34]. Therefore, the mechanism for the electrocatalytic oxidation of nitrite on the G/Pd/RGO modified GCE can be deduced as follows [35-37]: The interaction between nitrite and Pd/RGO to form a complex of Pd/RGO($NO_2$) (equation 1). The formation of $NO_2$ by losing one electron (equation 2) is followed by the disproportionation of the nitrogen dioxide to give nitrite and nitrate (equations 3 and 4). Nitrate is the sole product.

$$\mathrm{Pd/RGO} + \mathrm{NO_2^-} \rightleftharpoons [\mathrm{Pd/RGO(NO_2^-)}] \quad (1)$$

$$[\mathrm{Pd/RGO(NO_2^-)}] \rightleftharpoons \mathrm{Pd/RGO} + \mathrm{NO_2} + e^- \quad (2)$$

$$2\mathrm{NO_2} + \mathrm{H_2O} \rightleftharpoons 2\mathrm{H^+} + \mathrm{NO_3^-} + \mathrm{NO_2^-} \quad (3)$$

$$\mathrm{NO_2^-} + \mathrm{H_2O} \rightleftharpoons 2\mathrm{H^+} + \mathrm{NO_3^-} + 2e^- \quad (4)$$

### 3.3 *Optimization of the performance of nitrite sensors*

Figure 5B depicts the influence of pH (in the range of 3.0-8.0) on the anodic peak current response. The results show that the peak current increases slowly with increasing pH and reaches a maximum at pH 7.0. Further increasing pH to 8.0 decreases the current response. This result is well in accordance with previous reports [1, 38-40]. The cause of relatively low current response at acidic medium may be due to the following transformation of nitrite to NO and $NO_3^-$ [41]:

$$2\mathrm{H^+} + 3\mathrm{NO_2^-} \rightarrow 2\mathrm{NO} + \mathrm{NO_3^-} + \mathrm{H_2O}$$

On the other hand, the lack of proton in higher pH conditions will also affect the current response because the oxidation of nitrite is a proton dependent process [42]. Moreover, the oxide layer formed at the electrode surface under high pH conditions would inhibit the oxidation process [43]. Therefore, pH 7.0 has been chosen for measuring the nitrite.

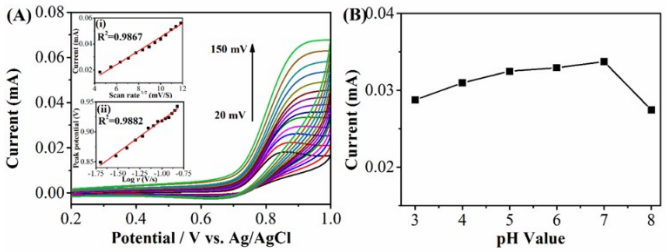


Figure 5. (A) Cyclic voltammograms of G/Pd/RGO in 0.1 M PBS containing 1 mM nitrite at different scan rates. Inset (i) is the linear dependence of the anodic peak current on the square root of the scan rate. Inset (ii) is the plot of peak potential vs. logarithm of scan rate. (B) The effect of pH on the current response of 1 mM nitrite at G/Pd/RGO electrode.

### 3.4. *DPV determination of nitrite*

DPV is a more sensitive technique than cyclic voltammetry and has been widely used for electrochemical analysis [44]. Figure 6A depicts the DPV curves of the G/Pd/RGO-3 electrode in various concentrations of nitrite from 1 to 1500 μM. As shown in Figure 6A, the DPV curves exhibit well-defined peaks corresponding to the oxidation of nitrite. The peak current increases linearly with the concentration of nitrite in the range of 1 to 1000 μM (Figure 6B). The corresponding regression equation is: $I$ (μA)= 0.02106 $C$(μM) + 0.34236 ($R^2$ = 0.9912). The detection limit was calculated to be 0.23 μM (S/N = 3). The analytical performances of G/Pd/RGO-3 are compared with other nitrite sensors in the literature and the results are shown in Table S1. Considering the simple electrode fabrication process, wide linear calibration range, high sensitivity and low detection limit, the G/Pd/RGO electrode can be used for practical detection of $NO_2^-$.

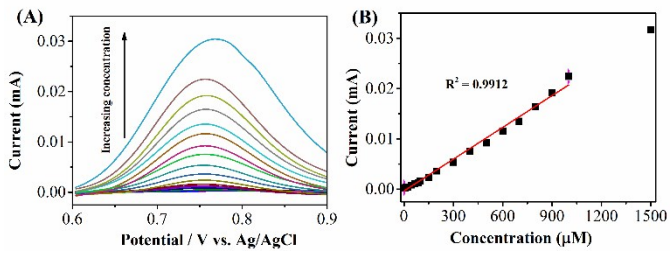


Figure 6. (A) Differential pulse voltammograms of the G/Pd/RGO-3 electrode in pH 7.0 solutions containing 1, 2, 5, 15, 25, 45, 65, 85, 100, 150, 200, 300, 400, 500, 600, 700, 800, 900, 1000 and 1500 μM nitrite. (B) The plot of $I_{pa}$ vs. the concentration of nitrite.

### 3.5. *Selectivity, reproducibility and stability*

The reproducibility of the proposed sensor towards the detection of nitrite was investigated. Figure S5 shows the eight repetitive DPV measurements of 1 mM nitrite using a same G/Pd/RGO-3 electrode. The RSD of the measurement is 2.07%. For the same nitrite solution, the RSD of measurement using six different G/Pd/RGO-3 electrodes is determined to be 2.56% (Figure S6). The results indicate that the stepwise fabrication method is very consistent for preparing Pd/RGO electrodes with reproducible results. The operational stability of proposed sensor was evaluated under hydrodynamic conditions. As shown in Figure S7 inset, the G/Pd/RGO-3 remains more than 94% of its initial response after one hour continuous measurement, indicating the proposed sensor owing an excellent operational stability.

The selectivity of the nitrite sensor was investigated by the detection of nitrite in the presence of some common interferences including ions and biological molecules. Current was measured under a constant potential of 0.8 V. As shown in Figure S7, no apparent interference was observed in the presence of 10-fold excess of $K^+$, $Na^+$, $Zn^{2+}$, $SO_4^{2-}$, $CO_3^{2-}$, $NH_4^+$ and $HPO_4^{2-}$, and 5-fold excess of biological interference including glucose, dopamine, uric acid and ascorbic acid, due to their low electro-activity at the applied potential. Thus, the stepwisely fabricated G/Pd/RGO electrode can be used for selective detection of nitrite in the presence of many common interference agents.

## 4. Conclusions

In this study, the RGO and Pd nanoparticles were successively deposited on a GCE via a novel stepwise electroless deposition method. This process is fast and can be repeated to achieve the desired amount of nanocomposite deposited on the electrode. UV-vis spectra confirmed the successful stepwise deposition process and nearly equal amount of materials were deposited on the electrode for each cycle. SEM images revealed the well separation of RGO sheets layers due to the insertion of Pd NPs. By combining the benefits of RGO and Pd nanoparticles, the resulting G/Pd/RGO composite electrode showed a much higher electrocatalytic performance towards the oxidation of nitrite than that of bare GCE, G/Pd and G/RGO. The proposed nitrite sensor exhibited a linear detection range between 1 to 1000 μM with a detection limit of 0.23 μM. Moreover, the constructed sensor is highly selective for nitrite determination, with excellent repeatability and stability.

**Acknowledgments**
Swinburne University Postgraduate Research Award (SUPRA) and the National Natural Science Foundation of China (21475033) are acknowledged for partially supporting this work.

## Notes and references

[a] *Department of Chemistry and Biotechnology, Faculty of Science, Engineering and Technology, Swinburne University of Technology, Hawthorn VIC 3122, Australia*
[b] *Division of Nanomaterials and Chemistry, Hefei National Laboratory for Physical Sciences at Microscale, Department of Chemistry, University of Science and Technology of China, Hefei , Anhui 230026 , P. R. China*
*Corresponding author: Aimin Yu; email: aiminyu@swin.edu.au*

## Reference

1. Y. Li, H. Wang, X. Liu, L. Guo, X. Ji, L. Wang, D. Tian and X. Yang, *Journal of Electroanalytical Chemistry*, 2014, **719**, 35-40.
2. K. Calfumán, M. J. Aguirre, P. Cañete-Rosales, S. Bollo, R. Llusar and M. Isaacs, *Electrochimica Acta*, 2011, **56**, 8484-8491.
3. N. Pourreza, M. R. Fat'hi and A. Hatami, *Microchemical Journal*, 2012, **104**, 22-25.
4. Z. Lin, W. Xue, H. Chen and J.-M. Lin, *Analytical Chemistry*, 2011, **83**, 8245-8251.

5. U. P. Azad, S. Turllapati, P. K. Rastogi and V. Ganesan, *Electrochimica Acta*, 2014, **127**, 193-199.
6. B. Yuan, C. Xu, L. Liu, Y. Shi, S. Li, R. Zhang and D. Zhang, *Sensors and Actuators B: Chemical*, 2014, **198**, 55-61.
7. A. Afkhami, F. Soltani-Felehgari, T. Madrakian and H. Ghaedi, *Biosensors & Bioelectronics*, 2014, **51**, 379-385.
8. J. R. C. da Rocha, L. Angnes, M. Bertotti, K. Araki and H. E. Toma, *Analytica Chimica Acta*, 2002, **452**, 23-28.
9. L. Fu, G. Lai, P. J. Mahon, J. Wang, D. Zhu, B. Jia, F. Malherbe and A. Yu, *RSC Advances*, 2014, **4**, 39645-39650.
10. R. L. McCreery, *Chemical Reviews*, 2008, **108**, 2646-2687.
11. S. N. Kim, J. F. Rusling and F. Papadimitrakopoulos, *Adv. Mater.*, 2007, **19**, 3214-3228.
12. L. Fu, J. Yong, G. Lai, T. Tamanna, S. Notley and A. Yu, *Materials and Manufacturing Processes*, 2014, **29**, 1030-1036.
13. L. Fu, G. Lai, H. Zhang and A. Yu, *Journal of Nanoscience and Nanotechnology*, 2015, **15**, 4325-4331.
14. A. Yu, X. Zhang, H. Zhang, D. Han and A. R. Knight, *Electrochimica Acta*, 2011, **56**, 9015-9019.
15. Y. Wang, Y. Li, L. Tang, J. Lu and J. Li, *Electrochemistry Communications*, 2009, **11**, 889-892.
16. S. Alwarappan, A. Erdem, C. Liu and C.-Z. Li, *J. Phys. Chem. C*, 2009, **113**, 8853-8857.
17. S. Palanisamy, S. Ku and S.-M. Chen, *Microchim Acta*, 2013, **180**, 1037-1042.
18. H. Zhou, Y. Liu, W. Chi, C. Yu and Y. Yu, *Appl. Surf. Sci.*, 2013, **282**, 181-185.
19. L. Fu and A. Yu, *Nanoscience and Nanotechnology Letters*, 2015, **7**, 147-151.
20. Z. H. Chen, J. S. Jie, L. B. Luo, H. Wang, C. S. Lee and S. T. Lee, *Nanotechnology*, 2007, **18**.
21. D. Li, M. B. Muller, S. Gilje, R. B. Kaner and G. G. Wallace, *Nat. Nano*, 2008, **3**, 101-105.
22. V. G. Plotnikov, V. A. Smirnov, M. V. Alfimov and Y. M. Shul'ga, *High Energy Chem.*, 2011, **45**, 411-415.
23. X.-L. Hou, J.-L. Li, S. C. Drew, B. Tang, L. Sun and X.-G. Wang, *J. Phys. Chem. C*, 2013, **117**, 6788-6793.
24. F. Tuinstra and J. L. Koenig, *The Journal of Chemical Physics*, 1970, **53**, 1126-1130.
25. X. Zhou, T. Shi and H. Zhou, *Appl Surf Sci*, 2012, **258**, 6204-6211.
26. S. Stankovich, D. A. Dikin, R. D. Piner, K. A. Kohlhaas, A. Kleinhammes, Y. Jia, Y. Wu, S. T. Nguyen and R. S. Ruoff, *Carbon*, 2007, **45**, 1558-1565.
27. P. Xi, F. Chen, G. Xie, C. Ma, H. Liu, C. Shao, J. Wang, Z. Xu, X. Xu and Z. Zeng, *Nanoscale*, 2012, **4**, 5597-5601.
28. X. Yan, J. Chen, J. Yang, Q. Xue and P. Miele, *ACS Applied Materials & Interfaces*, 2010, **2**, 2521-2529.
29. M. A. Kamyabi and F. Aghajanloo, *Journal of Electroanalytical Chemistry*, 2008, **614**, 157-165.
30. W. Si, W. Lei, Y. Zhang, M. Xia, F. Wang and Q. Hao, *Electrochimica Acta*, 2012, **85**, 295-301.
31. L. Chen, C. Yuan, H. Dou, B. Gao, S. Chen and X. Zhang, *Electrochimica Acta*, 2009, **54**, 2335-2341.
32. E. Laviron, *J. Electroanal. Chem.*, 1979, **101**, 19-28.
33. E. Laviron, *J. Electroanal. Chem.*, 1974, **52**, 355-393.
34. A. Afkhami, M. Bahram, S. Gholami and Z. Zand, *Analytical Biochemistry*, 2005, **336**, 295-299.
35. P. Li, Y. Ding, A. Wang, L. Zhou, S. Wei, Y. Zhou, Y. Tang, Y. Chen, C. Cai and T. Lu, *ACS applied materials & interfaces*, 2013, **5**, 2255-2260.
36. P. Tau and T. Nyokong, *Electrochimica Acta*, 2007, **52**, 4547-4553.
37. Y.-Y. Wu, C. Li, Z.-Y. Dou, L.-L. Cui, D.-J. Liu and X.-Q. He, *Journal of Solid State Electrochemistry*, 2014, **18**, 2625-2635.
38. D. Gligor and A. Walcarius, *Journal of Solid State Electrochemistry*, 2014, **18**, 1519-1528.
39. D. Ning, H. Zhang and J. Zheng, *Journal of Electroanalytical Chemistry*, 2014, **717-718**, 29-33.
40. L. Zhou, J.-P. Wang, L. Gai, D.-J. Li and Y.-B. Li, *Sensors and Actuators B: Chemical*, 2013, **181**, 65-70.
41. O. Brylev, M. Sarrazin, L. Roué and D. Bélanger, *Electrochimica Acta*, 2007, **52**, 6237-6247.
42. A. Afkhami, T. Madrakian, A. Shirzadmehr, M. Tabatabaee and H. Bagheri, *Sensors and Actuators B: Chemical*, 2012, **174**, 237-244.
43. B. Piela and P. K. Wrona, *Journal of The Electrochemical Society*, 2002, **149**, E55-E63.
44. L. Wu, L. Feng, J. Ren and X. Qu, *Biosensors and Bioelectronics*, 2012, **34**, 57-62.



 